Protein Science (2000), *9*:512–524. Cambridge University Press. Printed in the USA.

Analysis of the dynamic properties of *Bacillus circulans* xylanase upon formation of a covalent glycosyl-enzyme intermediate

GREGORY P. CONNELLY,[1] STEPHEN G. WITHERS,[1,2] AND LAWRENCE P. MCINTOSH[1,2]

[1]Department of Biochemistry and Molecular Biology, University of British Columbia, Vancouver, British Columbia, V6T 1Z3, Canada
[2]Department of Chemistry, The Protein Engineering Network of Centres of Excellence, University of British Columbia, Vancouver, British Columbia V6T 1Z3, Canada

(RECEIVED June 8, 1999; FINAL REVISION January 3, 2000; ACCEPTED January 18, 2000)

Abstract

NMR spectroscopy was used to search for mechanistically significant differences in the local mobility of the main-chain amides of *Bacillus circulans* xylanase (BCX) in its native and catalytically competent covalent glycosyl-enzyme intermediate states. ^{15}N T_1, T_2, and ^{15}N{^{1}H} NOE values were measured for ~120 out of 178 peptide groups in both the apo form of the protein and in BCX covalently modified at position Glu78 with a mechanism-based 2-deoxy-2-fluoro-β-xylobioside inactivator. Employing the model-free formalism of Lipari and Szabo, the measured relaxation parameters were used to calculate a global correlation time (τ_m) for the protein in each form (9.2 ± 0.2 ns for apo-BCX; 9.8 ± 0.3 ns for the modified protein), as well as individual order parameters for the main-chain NH bond vectors. Average values of the order parameters for the protein in the apo and complexed forms were $S^2 = 0.86 \pm 0.04$ and $S^2 = 0.91 \pm 0.04$, respectively. No correlation is observed between these order parameters and the secondary structure, solvent accessibility, or hydrogen bonding patterns of amides in either form of the protein. These results demonstrate that the backbone of BCX is well ordered in both states and that formation of the glycosyl-enzyme intermediate leads to little change, in any, in the dynamic properties of BCX on the time scales sampled by ^{15}N-NMR relaxation measurements.

Keywords: glucanase; glycosyl-enzyme intermediate; NMR; order parameter; protein structure; relaxation dynamics

Protein molecules undergo a wide variety of internal motions on timescales ranging from picoseconds to seconds or even longer. These motions may play an important role in the ability of proteins to perform their manifold functions, including catalysis and ligand binding. A major goal of current enzymology is to describe the structural and dynamic changes that enzymes undergo along their reaction pathways. Several recent studies have concluded that intramolecular motions are necessary for certain enzymes to catalyze their respective reactions, both in terms of substrate binding and the subsequent chemical and dissociation steps (Akke et al., 1993; Mandel et al., 1995; Stivers et al., 1996). However, good model systems involving small enzymes that can be trapped in intermediate states and subjected to analysis by NMR or X-ray crystallography are limited in number. One possible model system is the xylanase from *Bacillus circulans* (BCX).

Xylanases are an important class of enzymes that bind and hydrolyze xylan, a major component of plant cell walls. Numerous potential applications in the food preparation and pulp and paper industries have stimulated a widespread effort to investigate the process of xylan degradation in detail. BCX and several highly related Family 11/G xylanases have emerged as model β-glycosidases, being extensively characterized both structurally (Campbell et al., 1993; Törrönen et al., 1994; Törrönen & Rouvinen, 1995; Krengel & Dijkstra, 1996; McIntosh et al., 1996; Plesniak et al., 1996a, 1996b; Connelly & McIntosh, 1998) and functionally (Miao et al., 1994; Wakarchuk et al., 1994a, 1994b; Lawson et al., 1996, 1997; White et al., 1996; Törrönen & Rouvinen, 1997; White & Rose, 1997). The overall fold of BCX resembles a closed right-handed fist, with the active site cleft covered over by a loop or "thumb" region.

BCX is a retaining glycosidase (Gebler et al., 1992), cleaving xylan via a double-displacement mechanism involving a covalent glycosyl-enzyme intermediate that is formed by the nucleophilic attack of the carboxylate of Glu78 at the substrate anomeric center (Miao et al., 1994). This intermediate is formed and hy-

Reprint requests to: Lawrence P. McIntosh, Department of Biochemistry and Molecular Biology, University of British Columbia, Vancouver, British Columbia V6T 1Z3, Canada; e-mail: mcintosh@otter.biochem.ubc.ca.

Abbreviations: 2FXb, 2-deoxy-2-fluoro-β-xylobioside; 2FXb-BCX, BCX covalently modified at position Glu78 with 2-deoxy-2-fluoro-β-xylobioside; apo-BCX, unmodified BCX; BCX, *Bacillus circulans* xylanase; CPMG, Carr-Purcell-Meiboom-Gill; DNP-2FXb, 2,4-dinitrophenyl-2-deoxy-2-fluoro-β-xylobioside; HSQC, heteronuclear single quantum coherence spectroscopy; NOE, nuclear Overhauser effect; RMSD, root-mean-square deviation.

drolyzed via transition states with substantial oxocarbenium ion character and thus can be trapped by use of substrates such as 2,4-dinitrophenyl-2-deoxy-2-fluoro-β-xylobioside (DNP-2FXb). The fluorine at the C-2 position of this compound destabilized the positively charged transition states, while the good 2,4-dinitrophenolate leaving group ensures that glycosylation remains faster than deglycosylation. Although eventually hydrolyzed, the 2-deoxy-2-fluoroxylobiosyl-enzyme intermediate (2FXb-BCX) has a half-life of ~6 h at 40 °C and pH 6.0, indicating that deglycosylation is slowed by more than six orders of magnitude relative to the case with natural substrates (Miao et al., 1994). The catalytic competence of the intermediate is further demonstrated by its turnover via transglycosylation to an added acceptor sugar (Miao et al., 1994). Therefore, the 2FXb-BCX species is a valid model of an enzyme-intermediate complex. It is intriguing that studies of equivalent fluoroglycosyl-enzyme intermediates have revealed that such covalent modification of these glycosidases significantly increases their resistance to proteolytic cleavage (Street et al., 1992). However, subsequent crystallographic studies have detected very few substantial changes in three-dimensional structure upon intermediate formation (White et al., 1996; Burmeister et al., 1997; Davies et al., 1998; Notenboom et al., 1998; Sidhu et al., 1999). Differences in protease susceptibility may, therefore, arise from changes in the stability or dynamic properties of the enzyme upon formation of the glycosyl-enzyme intermediate.

This work is part of a series of studies on BCX aimed at elucidating the structural, dynamic, and electrostatic properties of the protein along its catalytic pathway. Structures of the native enzyme, a noncovalent Michaelis complex, and the glycosyl-enzyme intermediate of BCX have been solved by X-ray crystallography (Campbell et al., 1993; Wakarchuk et al., 1994a; Sidhu et al., 1999). These studies have revealed the basis of the specificity of BCX for xylan derivatives and highlighted the significant distortion of the proximal xylose ring upon formation of the 2-fluoro-xylobiosyl-enzyme intermediate. This distortion, along with numerous sugar–protein hydrogen-bonding interactions, likely stabilizes the transition states for both glycosylation and deglycosylation. ^{13}C-NMR titrations of the apo protein have revealed pK_a values of 4.6 and 6.7 for Glu78 and Glu172, respectively (McIntosh et al., 1996), demonstrating that at the enzyme's pH optimum of 5.7, the nucleophile Glu78 is deprotonated while the general acid Glu172 is protonated. Remarkably, the pK_a of Glu172 drops to 4.2 upon formation of the 2-fluoro-xylobiosyl-enzyme intermediate, allowing Glu172 to function as a general base in the deglycosylation step. This "pK_a cycling" is attributed in part to the loss of the negative charge of Glu78 upon formation of the glycosyl-enzyme intermediate, and thus is intrinsic to the double displacement mechanism of BCX (McIntosh et al., 1996).

In this study we use ^{15}N-relaxation dynamics measurements on both apo-BCX and 2FXb-BCX to address the question of whether the flexibility of the backbone of the enzyme changes along its catalytic pathway. We report the order parameters for the amide NH bond vectors of BCX, both in the unbound form (apo-BCX) and in complex with the inactivator (2FXb-BCX). On the whole, the S^2 values for apo-BCX are uniformly high (average $S^2 = 0.86 \pm 0.04$), showing little variation with secondary structure or other structural parameters such as amide hydrogen bonding or solvent-exposed surface area. The average order parameter increases only marginally in 2FXb-BCX to a value of $S^2 = 0.91 \pm 0.04$, indicating that formation of the glycosyl-enzyme intermediate leads to little, if any, change in the dynamic properties of BCX on the time scales sampled by ^{15}N relaxation measurements. Thus, any increase in the global stability of the enzyme or in its resistance proteolysis due to covalent modification is not reflected by the motions of the protein occurring on a subnanosecond timescale.

Results

Assignment of the NMR spectrum of 2FXb-BCX

Figure 1 shows the ^{1}H–^{15}N HSQC spectrum of 2FXb-BCX. We assigned the cross peaks in this spectrum using the same strategy previously employed for apo-BCX (Plesniak et al., 1996b). Specifically, the HNCACB and CBCA(CO)NH experiments were exploited to provide scalar correlations between resonances from the backbone $^1H^N$ and ^{15}N nuclei of each amide with the $^{13}C^\alpha$ and $^{13}C^\beta$ nuclei from its own residue and those from the preceding amino acid (Grzesiek & Bax, 1992; Wittekind & Müeller, 1993). In most instances, both the inter- and intraresidue connections between the $^{13}C^\alpha$ and $^{13}C^\beta$ and the amide $^1H^N$ of each amino acid were observed in the HNCACB experiment, thus allowing the unambiguous connection of spin systems from neighboring residues. Following this approach, the ^{1}H and ^{15}N resonances of 177 out of 179 nonproline residues were assigned. The only exceptions were Ala1, which has no amide, and Ser2, for which a signal was not detected (see Plesniak et al., 1996b). All NMR assignments have been submitted to the BioMagResBank.

Differences in $^1H^N$ and ^{15}N chemical shifts between apo-BCX and 2FXb-BCX are plotted as a function of residue number in Figure 2. Many of the smallest perturbations ($\Delta\delta < 0.05$ ppm for $^1H^N$ and $\Delta\delta < 0.2$ ppm for ^{15}N) are attributable to the slight change in pH and ionic strength resulting from addition of DNP-2FXb. However, there are several regions of the protein where clusters of residues experience more pronounced chemical shift changes (e.g., $\Delta\delta > 0.2$ ppm for $^1H^N$ and $\Delta\delta > 1.0$ ppm for ^{15}N). When these perturbations are mapped onto the three-dimensional structure of BCX, as shown in Figure 3A, it is apparent that most of the largest differences occur for residues that line the binding cleft and form the thumb region. In contrast, there are no large chemical shift changes in amides that are distal from the binding site. This clearly indicates that any structural changes, which occur in the backbone of BCX as a result of covalent modification of Glu78, are localized to the binding site itself.

^{15}N T_1, T_2, and ^{15}N{^{1}H} NOE measurements and calculation of τ_m

The T_1, T_2, and heteronuclear NOE data for apo-BCX and 2FXb-BCX are plotted as a function of residue number in Figure 4. High-quality relaxation data were acquired for 128 peptide NH groups in apo-BCX and 117 for 2FXb-BCX. Data for the remaining residues were discarded due to spectral overlap or poor fits to a single exponential decay. The average T_1 value for all backbone amides increased slightly from 564 ± 26 ms for apo-BCX to 583 ± 28 ms for the protein in the complex. However, the average T_2 value showed a decrease from 88 ± 7 ms for apo-BCX to 81 ± 6 ms for 2FXb-BCX. The average ^{15}N{^{1}H} NOE measured for each peptide group was also slightly higher for the protein in the complex, increasing from 0.73 ± 0.05 to 0.76 ± 0.03.

Using the measured relaxation parameters, a global correlation time (τ_m) was calculated for both apo-BCX and 2FXb-BCX (Far-

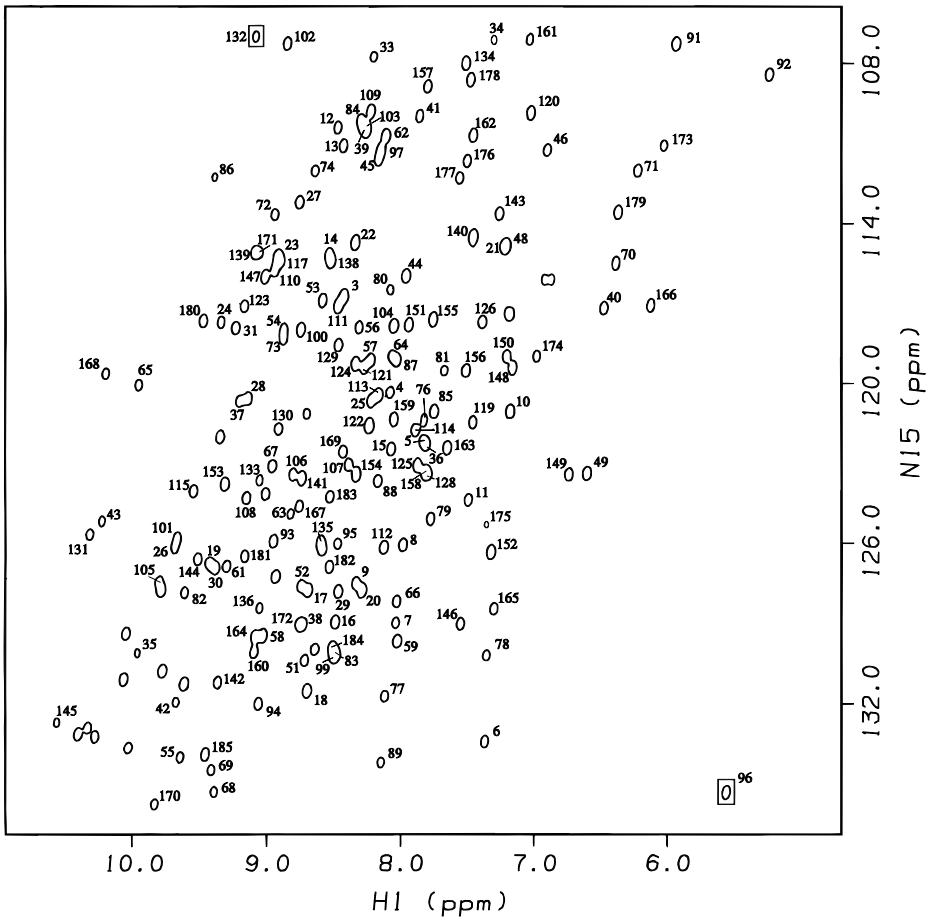

Fig. 1. ^{1}H–^{15}N HSQC spectrum of uniformly $^{13}C/^{15}N$-enriched BCX covalently bonded to 2FXb. Cross peaks for Gly96 and Arg132 (boxed) have ^{15}N shifts that are outside the spectral window and are thus aliased and inverted in the spectrum. The cross peak for Ile118, with H^N and ^{15}N shifts of 4.00 and 108.8 ppm, respectively, is not shown. Signals from the side-chain $N^{\delta}H$ and $N^{\epsilon}H$ of Asn and Gln residues are not detected due to the use of a refocused INEPT within the T_1 pulse sequence used to record this spectrum. The indole $N^{\epsilon 1}H$ cross peaks from the tryptophan residues and the $N^{\epsilon}H$ cross peaks from the arginines in BCX are not assigned. (See Fig. 1 of Plesniak et al., 1996b, for the HSQC of apo-BCX.)

row et al., 1994). Data from residues whose T_1/T_2 ratio differed by more than one standard deviation from the average were not included at this stage. τ_m for apo-BCX was 9.2 ± 0.2 ns, while for 2FXb-BCX it was 9.8 ± 0.3 ns. These values are consistent with the observed general increase in T_1 and NOE values and the decrease in T_2 values for 2FXb-BCX relative to apo-BCX, and indicate that the protein is in the slow-tumbling regime under the experimental conditions (Kay et al., 1989; Peng & Wagner, 1992a, 1992b).

Relaxation dynamics of Apo-BCX

The S^2 values calculated for apo-BCX according to the isotropic Lipari and Szabo (1982a, 1982b) formalism are displayed in Figure 5, along with any accompanying parameters for residues whose relaxation data were best fit with one of the more complex models (for an explanation of the various relaxation models, see the Materials and methods). Table 1 shows that nearly one-half of the residues whose relaxation parameters were analyzed (60 of 125) required one of the more complex models incorporating chemical exchange terms or motions on two widely different time scales (models 3, 4, or 5) to adequately describe their behavior. Nevertheless, the average order parameter for the peptide NH bond vectors in the apo form of BCX is quite high ($S^2 = 0.86 \pm 0.04$), indicating that, in general, the main-chain atoms are motionally restricted in the folded protein on a pico-nanosecond time scale. These relaxation data are thus consistent with crystallographic and hydrodynamic (Plesniak et al., 1996b) studies, which reveal that BCX is a very compact, globular molecule.

Table 1. *Number of residues in apo-BCX and 2FXb-BCX fit to each relaxation model*

Model	(Parameters)	Apo-BCX	2FXb-BCX
1	(S^2)	11	28
2	(S^2, τ_e)	54	59
3	(S^2, R_{ex})	3	4
4	(S^2, τ_e, R_{ex})	25	8
5	(S^2, S_f^2, τ_s)	32	11

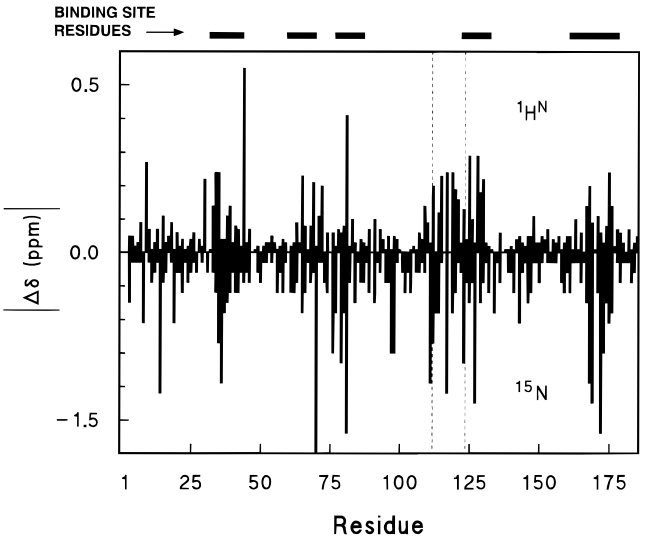

Fig. 2. Perturbations of the main-chain $^1H^N$ and ^{15}N chemical shifts of BCX upon covalent modification with 2FXb. For simplicity, proton chemical shift differences are all plotted as positive absolute values, while the nitrogen differences are plotted as negative absolute values. The pattern of chemical shift changes confirms that the 2FXb moiety is covalently bonded within the active site of BCX. The residues lining the binding site are indicated by the heavy black bars at the top of the panel, and the residues between the dotted lines comprise the thumb region of BCX.

Figure 3B illustrates the calculated order parameters mapped onto the structure of the free protein. Only slight variations in these values are seen with secondary structure, with amides in the single helix having marginally higher S^2 values that those in β-strands (Table 2). Of the 14 residues with $S^2 \leq 0.80$, Val16, Ala18, Ser22, Gly56, Trp58, and Ser179 lie within the β-sheet distal to the active site cleft, Asn8, Lys40, Thr126 in the β-sheet surrounding this cleft, Ile118, Asp121, Arg122 within the thumb region, and Thr3 and Gly161in regions of nonregular secondary structure. The only trend that emerges from this small collection of residues, which exhibit slightly lower order parameters than the global average, is a clustering within the outermost β-strand of the distal β-sheet (residues 15–22, $S^2 = 0.78 \pm 0.04$) and within the thumb region (residues 113–124, $S^2 = 0.82 \pm 0.06$). Finally, no correlation was observed between measured S^2 values and the solvent accessible surface area of each peptide NH group or its crystallographic *B*-factor ($R^2 = 0.05$ and 0.08, respectively). The R^2 correlation coefficients are given for the molecule as a whole, but similar results were obtained when different elements of secondary structure were considered separately (data not shown).

Table 2. *Average order parameters for residues of apo-BCX and 2FXb-BCX in different types of secondary structure*

	Global	α-Helix	β-Sheet	Loops (all)	Thumb (Y113–T124)
Apo-BCX	0.86(4)[a]	0.90(3)	0.86(4)	0.84(5)	0.82(6)
2FXb-BCX	0.91(4)	0.94(2)	0.90(4)	0.91(5)	0.91(6)

[a]The standard deviation of the final digit for each value is shown in parentheses.

Relaxation dynamics of 2FXb-BCX

Upon formation of the glycosyl-enzyme intermediate, the average S^2 value for all residues in BCX increases slightly to 0.91 ± 0.04 (Fig. 5; Table 2). Relative to apo-BCX, residues throughout the protein show small changes in their order parameters, and almost all of these are in the positive direction. When mapped onto a ribbon diagam representing the structure of BCX (Fig. 3C), we find that residues showing increases in $S^2 \geq 0.08$ cluster somewhat within the single α-helix, in an extended region near residue 132–136, and in the thumb region (the latter having an average $S^2 = 0.91 \pm 0.06$ that is now equal to the global average for 2FXb-BCX). However, with the exception of the thumb region, the significance of these changes in terms of the effect of the inhibitor on the structure and dynamics of BCX is unclear, particularly since the magnitude of these changes is not much greater than the errors calculated for the order parameters themselves. In addition, several residues scattered throughout the protein display decreased S^2 values upon complex formation, again with changes near the error limit.

One difference between the data sets for apo-BCX and 2FXb-BCX is seen in the number of amides whose relaxation behavior can be adequately described by each of the models outlined in Materials and methods (see Table 1). Specifically, the number of residues whose relaxation dynamics are best fit with the simplest models (1 and 2), using only the variables S^2 or S^2 plus τ_e increases from 65 for apo-BCX to 87 for 2FXb-BCX. Conversely, the number of residues requiring the more complex models (3, 4, and 5) to be well fit decreases significantly from 60 in apo-BCX to 23 in 2FXb-BCX. Likewise, while 28 of the NH groups in apo-BCX show some evidence of chemical exchange broadening (models 3 and 4), only 12 show this behavior in the complex. Finally, residues 15–19, which lie on the outside of the first β-sheet, require the two-site model of relaxation (model 5) to describe their behavior in both forms of the protein. The average values for the other motional parameters (R_{ex}, S_f^2, and τ_s) are similar for the two forms of the protein, the difference being in the number of residues that require those parameters to fit their relaxation data.

Discussion

In this study we used NMR spectroscopy to probe the structural and dynamic consequences of covalently modifying BCX with DNP-2FXb. Together, the protein and this "slow substrate" form a stable, yet catalytically competent, glycosyl-enzyme intermediate, thereby effectively freezing the enzyme midway along its reaction pathway. This permits a comparison of the dynamic properties of BCX in its apo and covalent-intermediate states.

Structural analyses of apo- and 2FXb-BCX

To assess the structural perturbations that occur in BCX as a consequence of forming the glycosyl-enzyme intermediate, we compared the ^1H-^{15}N HSQC of apo- and 2FXb-BCX. Amide chemical shifts are exquisitely sensitive to local conformational changes, such as alterations in hydrogen bond geometry or changes in orientation with respect to aromatic side chains. Thus, they are difficult to interpret in an absolute structural sense. However, the

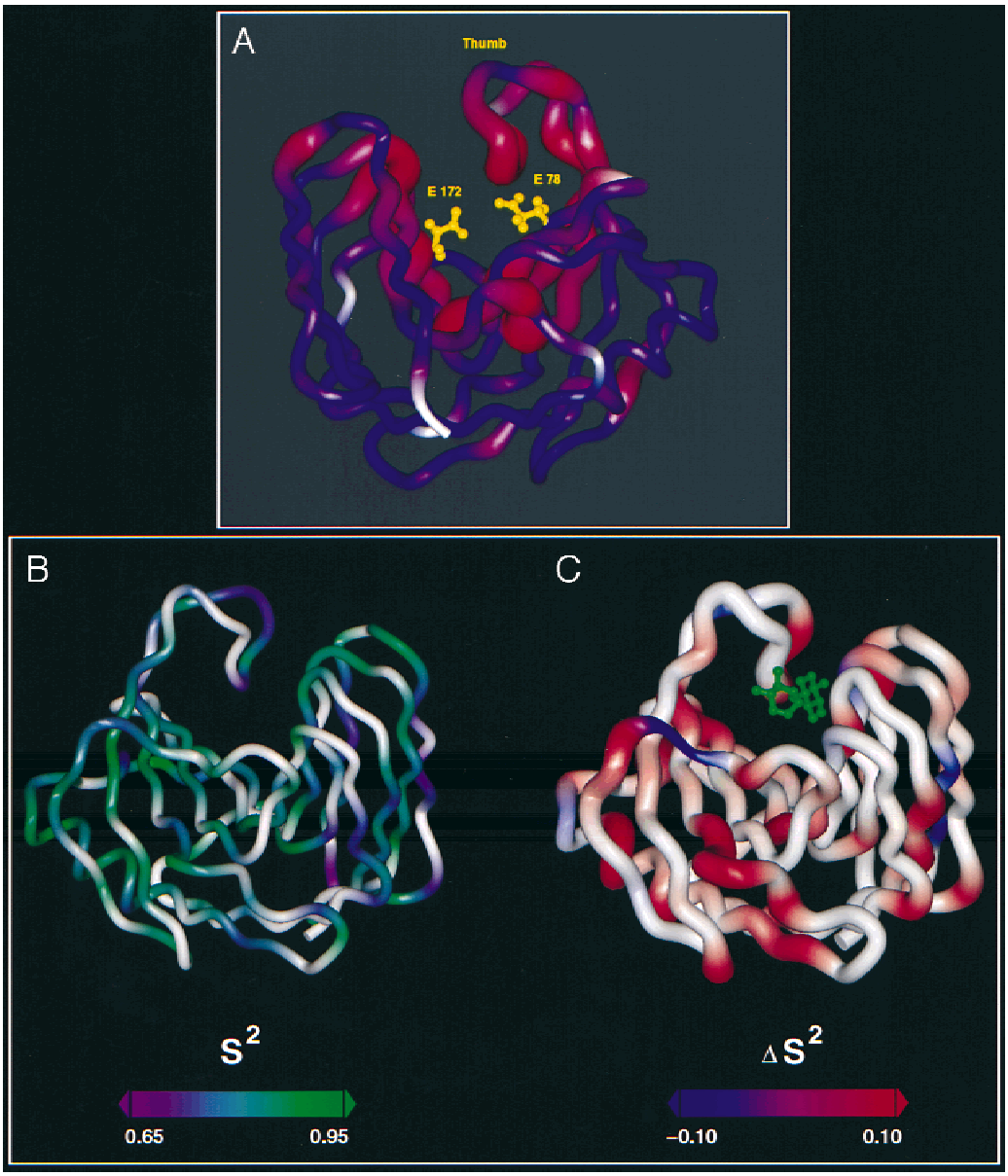

Fig. 3. **A:** Perturbations in the chemical shifts of the amides in BCX upon formation of the glycosyl-enzyme intermediate mapped on to the structure of the free enzyme (Campbell et al., 1993). The overall tertiary structure of the protein resembles a closed right fist, with a loop or "thumb" of residues lying over the active-site cleft where the two catalytic glutamic acid residues, Glu78 and Glu172, are located. Regions with the largest $^{1}H^{N}$ and ^{15}N chemical shift differences between the free and inhibitor-bound states are shaded red, while regions that experience little or no chemical shift changes with binding are colored blue. The white sections of the chain represent residues that have no peptide NH group (prolines, N-terminus). The width of the ribbon in this figure has also been drawn to reflect the same chemical shift changes (wider ribbon = larger $\Delta\delta$). Consistent with the covalent modification of the enzyme at Glu78, chemical perturbations are seen for residues lining the binding cleft. **B:** The calculated S^2 values for apo-BCX mapped on to the structure of the free enzyme. The main chain is shaded using a continuous color ramp, from purple ($S^2 = 0.65$) to green ($S^2 = 0.95$). White areas of the chain represent proline residues, or residues for which an order parameter could not be obtained due to spectral overlap or poor quality data. **C:** ΔS^2 values ($S^2_{\text{2FXb-BCX}}$-$S^2_{\text{apo-BCX}}$) of all residues for which an order parameter could be calculated for both forms of the protein. The data are represented on the crystal structure coordinates of the 2FXb-BCX complex (Sidhu et al., 1999), and the position of the covalently bonded xylobiose residue is shown in green. Red regions of the chain represent positive changes in S^2, blue regions represent negative changes, and white indicated prolines and residues for which order parameters were not obtained in one or both forms of the protein. The thickness of the chain is again drawn to indicate the relative magnitude of the changes.

pattern of perturbations we observe upon formation of the 2FXb-BCX species are wholly consistent with the structure of the inhibited enzyme obtained by X-ray crystallography (see Fig. 3A). Inspection of the crystal structure of 2FXb-BCX shows no significant structural rearrangements for backbone atoms relative to apo-BCX (0.2 Å RMSD between the two structures for all backbone atoms), except for a concerted displacement of the thumb region over the binding cleft (1.1 Å RMSD) (Campbell et al., 1993; Sidhu

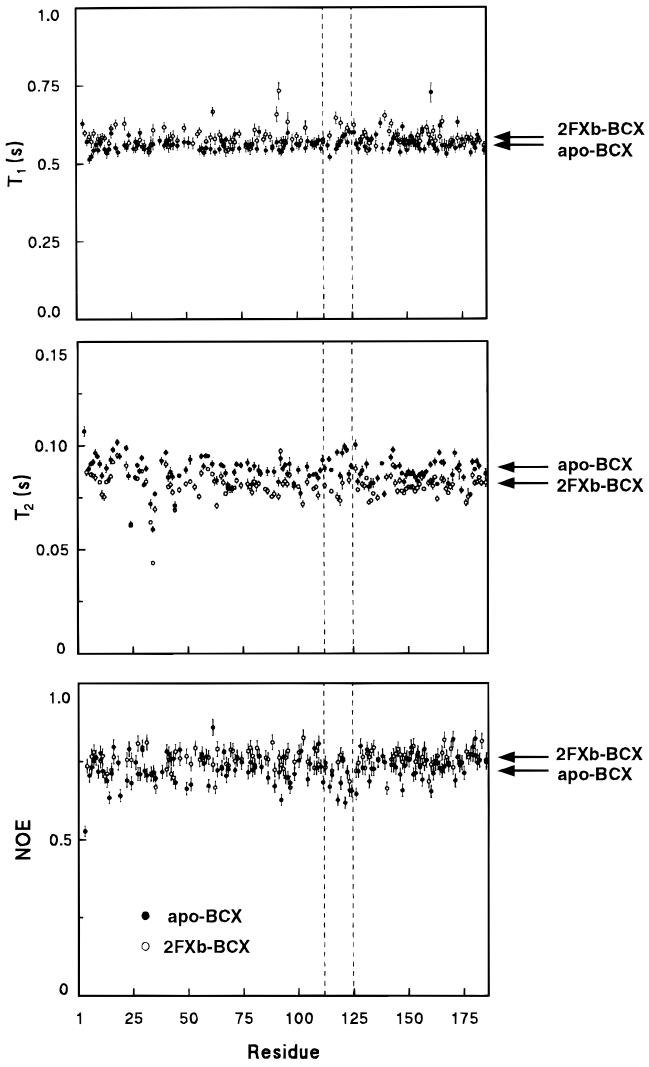

Fig. 4. ^{15}N T_1, T_2, and $^{15}N\{^1H\}$ NOE values for the main-chain amides of apo-BCX (filled circles) and 2FXb-BCX (open circles) at pH 5.7 and 30 °C. Residues forming the thumb region of BCX are enclosed between the dotted lines. The mean values for each quantity are indicated by the arrows on the right, and individual errors, which are on the order of 3% or less, are shown by error bars. Data for peptide groups whose HSQC signals were severely overlapped in either the free or the bound sample were discarded.

et al., 1999). We, therefore, conclude that the chemical shift changes observed for residues of BCX throughout the binding site reflect subtle structural perturbations that fall within the errors of the X-ray crystallographic analysis. By way of comparison, NMR studies on apo- and holo-coenzyme A binding protein have also shown numerous chemical shift differences upon complex formation, yet only small structural changes (Rischel et al., 1994). Similarly, single-site amino acid mutations in T4 lysozyme induce only minor overall structural perturbations in the molecule while giving rise to a much broader range of chemical shift variations (Anderson et al., 1993).

Previous studies of BCX have unambiguously demonstrated Glu78 to be the active-site nucleophile and Glu172 to be the acid/base catalyst (Miao et al., 1994; Wakarchuk et al., 1994a; McIntosh et al., 1996; Sidhu et al., 1999). Surprisingly, Glu78 experiences a change of only 0.1 ppm in its ^{15}N resonance, even though it becomes covalently modified in the intermediate. Glu172 shows a much larger chemical shift change of 1.8 ppm between apo-BCX and 2FXb-BCX. A similar pattern is seen for the ^1H chemical shift differences. This indicates that any chemical shift changes caused by intrinsic (through-bond), electrostatic, or structural perturbations are balanced out at the amide of Glu78. Nevertheless, amides adjacent to Glu78 are significantly perturbed in both $^1H^N$ and ^{15}N chemical shift, and the data in Figure 3A are consistent with the binding of 2FXb to this site in BCX.

Correlation times for global tumbling

The τ_m for the global tumbling of apo-BCX was extracted from the ^{15}N relaxation data. Using the measured value of 9.2 ns, we calculate a Stokes radius of 22.6 Å for the protein (Cavanagh et al., 1996). After correction for a hydration layer of ~3 Å, this value (19.6 Å) is slightly larger than that of ~18 Å estimated from the X-ray structure of the apoprotein. Similar discrepancies have been seen in other studies (Zink et al., 1994; Clubb et al., 1995; Kay et al., 1998) and probably reflect the fact that the calculated τ_m depends on the third power of the radius and, thus, is exquisitely sensitive to the exact molecular dimensions and degree of hydration of each given protein. Nevertheless, a τ_m of 9.2 ns is within the range expected for a 20 kDa protein existing in a predominantly monomeric form. This conclusion is supported by equilibrium and velocity sedimentation studies that unambiguously demonstrate that BCX is monomeric under the closely related conditions used for these particular measurements (Plesniak et al., 1996b).

Upon inactivation, the τ_m for 2FXb-BCX increased to 9.8 ns. Based solely on hydrodynamic considerations, this would reflect a 2% increase in the Stokes radius of the protein. Crystallographic analyses indicate that the structure of BCX does indeed expand slightly upon covalent modification due to the outward displacement of the thumb region by an RMSD of 1.1 Å (Campbell et al., 1993; Sidhu et al., 1999). It is difficult to judge whether this small conformational change is sufficient to account for the difference in τ_m values measured for apo- and 2FXb-BCX. However, it is noteworthy that relaxation dynamics studies of other protein–ligand and enzyme–substrate complexes have shown comparable increases in global tumbling times upon complex formation (Stivers et al., 1996; Olejniczak et al., 1997), but no clear explanation has been evinced. In the case of BCX, we note that the small increase in τ_m could, at least in part, also result from change in the ionic strength or pH of the solution due to the addition of DNP-2FXb. Specifically, the initial sample pH was 5.7, yet after addition of 2.0 mg of inhibitor it dropped to 5.4. Previous investigation of BCX (Plesniak et al., 1996b) suggested that the protein may weakly self-associate with increasing ionic strength, as evidenced by a decrease in the quality of its NMR spectra at elevated salt concentrations. As discussed below, theoretical studies indicate that such nonspecific association can result in an increased value of τ_m, as well as overestimation of the order parameters derived from use of the simple, isotropic Lipari and Szabo formalism (Schurr et al., 1994). Unfortunately, due to the very limited quantities of DNP-2FXb available for these studies, we were unable to measure these ^{15}N relaxation parameters as a function of protein concentration or buffer ionic strength and pH, in the attempt to distinguish whether the observed increase in τ_m resulted from the observed conformational change or from weak self-association.

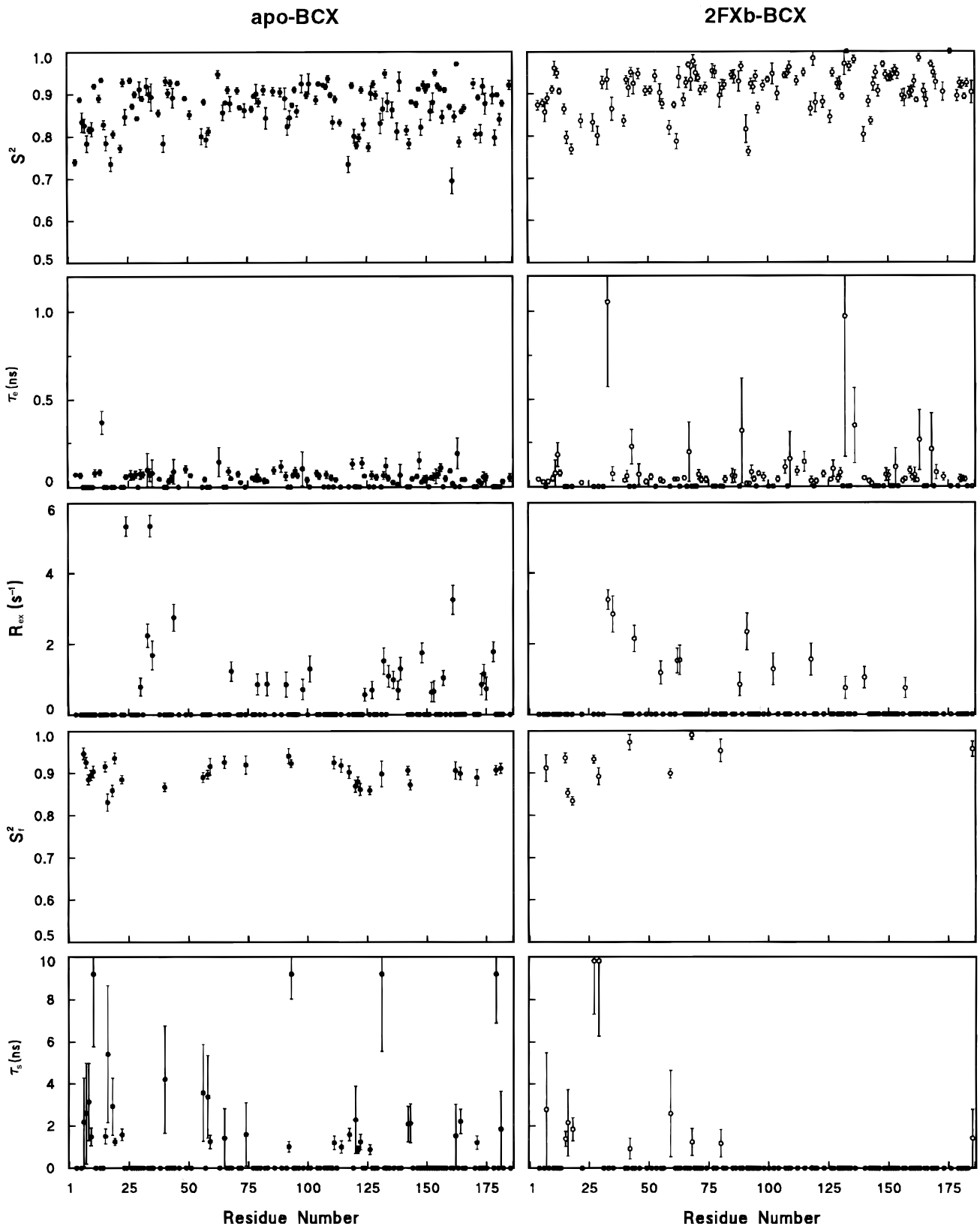

Fig. 5. ^{15}N dynamics data for apo-BCX (filled circles) and 2FXb-BCX (open circles). The correlation time (τ_m) for global tumbling was calculated to be 9.2 and 9.8 ns for the free protein and the complex, respectively. From top to bottom, the data are shown for S^2 (overall generalized order parameter), τ_e (time constant for fast motions), R_{ex} (rate for chemical exchange), S_f^2 (order parameter for fast motions, for residues that do not fit to one of the single-site models), and τ_s (time constant for these motions). For definitions of these quantities, see Table 1 and Materials and methods.

The correlation times reported for apo- and 2FXb-BCX were derived assuming isotropic tumbling of each molecule in solution. However, based on their high-resolution crystal structures, the calculated moments of inertia for apo-BCX (1.00:0.91:0.78) and the covalently modified glycosyl-enzyme intermediate (1.00:0.91:0.80) suggest a small degree of asymmetry. Therefore, we also attempted to analyze the measured relaxation data according to anisotropic models of rotational diffusion. Using the quadratic representation approach of Brüschweiler et al. (1995), both forms of the protein yielded values of $D_{\|}/D_{\perp} \sim 0.93$ when the ratios of their T_1 and T_2 lifetimes were fit to an axially symmetric model. However, only in the case of 2FXb-BCX was the fit to the observed relaxation data statistically better than that provided by the isotropic model, as judged by an *F*-test (Lee et al., 1997). In neither case was use of a fully anisotropic model warranted. Although this result is indicative of a small degree of nonisotropic tumbling for 2FXb-BCX, we have chosen to analyze the relaxation data for both forms of the protein by an isotropic model for several reasons. These include consistency sake, recognition of the observation of Blackledge et al. (1998) that multiple minima may exist when extracting axially symmetric diffusion parameters from ^{15}N relaxation data, and because an initial inclusion of anisotropic tumbling into the model free analysis did not appear to cause any significant changes in the order parameters or other relaxational terms derived for either apo- or 2FXb-BCX (not shown). This observation is consistent with previous reports that the description of the fast internal dynamics of a protein is relatively insensitive to the exact choice of a diffusion model (Schurr et al., 1994; Tjandra et al., 1995).

Fast internal dynamics of apo-BCX and 2FXb-BCX

The average values of the generalized order parameters determined for apo-BCX and 2FXb-BCX are high ($S^2 = 0.86 \pm 0.04$ and 0.91 ± 0.04, respectively), indicating that both forms of the protein are quite rigid in the pico-to-nanosecond regime under the experimental conditions used in this study. We seen only slight variations in these values with secondary structure (Table 2), and no correlation in either form of the enzyme between the calculated order parameters and structural features, such as peptide group solvent accessibility or hydrogen bonding. This uniformity is not unexpected given the extensive β-sheet structure of this xylanase and that, based on the program HBPLUS (McDonald & Thornton, 1994), backbone NH groups of 146 of the 185 residues in the crystal forms of both apo- and 2FXb-BCX participate in intramolecular hydrogen bonds.

Overall, the measured T_1, T_2, and NOE and derived S^2 values for the backbone amides in BCX do not vary significantly, even between residues in the nine strands of β-sheet vs. those in turns or loops (Table 2). In contrast, for many proteins order parameters for residues at the N- and C-termini or in exposed loop regions tend to be distinctly lower than those for the rest of the main chain (Akke et al., 1993; Mandel et al., 1995; Olejniczak et al., 1997). Indeed, in the most pronounced cases, measured ^{15}N{^{1}H} NOE values can even be negative, indicative of a high degree of conformational disorder. In contrast, the S^2 values at the amino- and carboxy-termini of BCX are typical of the other main-chain residues, indicating that the ends of the backbone are not motionally disordered. Inspection of the crystal structure reveals the likely explanation for this observation. Namely, the N- and C-termini are held together by a salt bridge between the NH_3^+ of Ala1 and the COO^- of Trp185, and both amino acids are part of the largest β-sheet in the molecule (Campbell et al., 1993; Joshi et al., 1997; Sidhu et al., 1999). These observations indicate that every part of the backbone participates in the organized tertiary structure of this bacterial xylanase. One exception to observation of generally uniform relaxation rates is seen with the anomalously low T_2 values, and hence, large R_{ex} terms (Fig. 5), measured for residues Thr33, Gly34, and Asn35 in both forms of the protein (Fig. 4). Inspection of the structure of BCX reveals no apparent reason for this unusual behavior as these residues appear very well ordered, following a β-turn linking internal strands of the two β-sheets in BCX.

Changes in fast dynamics upon covalent modification

Upon formation of the glycosyl-enzyme intermediate, the average S^2 value of all backbone amides in BCX increases marginally from 0.86 ± 0.04 to 0.91 ± 0.04. Given that the difference in average S^2 values is of the same order as the errors on each, and keeping in mind that the τ_m differed slightly between apo-BCX and 2FXb-BCX, the significance of this small increase is unclear. One possible interpretation is that this change may indeed reflect a very slight reduction in the fast internal dynamics of the whole protein due to covalent modification. However, alternative explanations exist. Neglect of possible anisotropic tumbling may influence the fitted order parameters, although this was not seen in a cursory analysis of the relaxation data when using an axially symmetric model. More plausibly, as noted above, if the increase in the τ_m value determined for 2FXb-BCX does reflects a small degree of nonspecific self-association, then fitting to the simple Lipari and Szabo formalism for isotropic tumbling could lead to artificially high S^2 values (Schurr et al., 1994). Therefore, within experimental limits, we must conclude that no significant changes were detected by ^{15}N relaxation methods in the overall dynamic properties of BCX upon formation of the glycosyl-enzyme intermediate. Given that apo-BCX is relatively rigid to begin with and shows no major variations in S^2 values along its backbone, the absence of any pronounced decrease in its mobility on a sub-nanosecond time regime, after modification with DNP-2FXb, is not unexpected. Note, however, these results also exclude the possibility of increased fast internal dynamics accompanying the covalent modification of BCX.

One segment of BCX that warrants closer inspection is the thumb region, located along the active site cleft of the enzyme (Fig. 3). As summarized in Table 2, the average order parameters of residues 113–124 in apo-BCX are slightly less than the global average for this form of the protein (0.82 ± 0.06 vs. 0.86 ± 0.04), yet equal to the global average for 2FXb-BCX (0.91 ± 0.06 vs. 0.91 ± 0.04). It is tempting to speculate that the thumb region exhibits marginally more mobility on a sub-nanosecond time scale than the remainder of apo-BCX, and that any difference in such mobility is lost upon glycosylation. For example, the S^2 value of Ile118, located at the tip of the thumb, increases from 0.74 in apo-BCX to 0.85 in 2FXb-BCX. Parenthetically, the amide of this isoleucine is hydrogen bonded to the aromatic ring of Trp71 (Plesniak et al., 1996b), and directly contacts the bound sugar in 2FXb-BCX. Unfortunately, reliable relaxation data for other residues within the thumb region, such as Gly120 and Asp121, which also show relatively low S^2 values in the apo-protein, could not be measured in the modified enzyme, thus limiting the reliability of this conclusion. Note also that, although appearing somewhat exposed in the ribbon diagrams of Figure 3, the thumb region is in fact very well structured as a classical hairpin, containing a Type I

β-turn (residues Ser117 to Gly120) and six internal hydrogen bonds. As with the rest of the protein, we observe no correlation between the measured order parameters and accessible surface area, hydrogen bonding, or crystallographic *B*-factors of the individual amide groups within this loop.

By way of comparison, the thumb region is the only portion of BCX showing a significant difference in placement between the crystal structures of the apo- and 2FXb-protein. Specifically, the thumb opens in a hinge-like fashion from the body of the enzyme by an RMSD of 1.1 Å to accommodate the substrate. This appears to result from noncovalent interactions between the distal sugar of the bound substrate and Pro116, Ser117, and Ile118 in the thumb and likely leads to the chemical shift perturbations highlighted in Figure 3A. Inspection of the structure of a noncovalent Michaelis complex of a catalytically inactive mutant form of BCX with xylotetraose reveals that the thumb is similarly shifted (Wakarchuk et al., 1994a), indicating that, indeed, it is the presence of the bound substrate that causes its displacement, rather than covalent bond formation per se. Interestingly, the structure of apo-BCX has also been solved in the $P2_12_12$ space group (G. Sidhu, unpubl. results). A comparison with the structure determined in the original $P2_12_12_1$ space group (Fig. 3) shows no significant differences except for a 0.6 Å RMS displacement of backbone atoms in the thumb. These residues form an interprotein contact in both crystal forms and thus their exact position within each space group is likely influenced by packing interactions. Extrapolating from these crystallographic results, it is reasonable to suggest that the thumb region in apo-BCX can undergo a hinge-bending motion to sample an ensemble of conformations in solutions. This motion may be reflected in the slightly lower order parameters derived for amides of the thumb region from the model free analysis of the measured ^{15}N relaxation data (Fig. 3B), although it could well occur on a timescale, such as that of the microsecond regime, not readily detected using this NMR approach. Note, however, because neither conformational exchange broadening (R_{ex} terms; Fig. 5) nor multiple resonances are observed in the ^{1}H or ^{15}N NMR spectra of residues forming the thumb, such postulated motions are unlikely to occur at any slower frequency.

Motions on other timescales

One difference between the relaxation behavior of apo- and 2FXb-BCX is seen in the number of amides that fit to the simple vs. complex isotropic models of protein dynamics. In general, residues that required more terms to accurately model their relaxation behavior (models 3, 4, and 5) in the apo state of the protein were often able to be fitted using one of the simpler models (1 and 2) after the intermediate was formed (see Table 1). This phenomenon has also been seen for other systems, including SH2 domains and ribonuclease H1 (Farrow et al., 1994; Mandel et al., 1995). One possible interpretation of this observation is that, in BCX, several residues in the apo-protein have mobility on the microsecond-to-millisecond timescale, which is dampened upon formation of the glycosyl-enzyme intermediate. In particular, for the span of residues 125–155, which lies just to the C-terminal side of the thumb region and contains six residues that line the binding cleft, we note that 11 NH groups require a chemical exchange term (R_{ex} in models 3 or 4) to model their relaxation behavior in apo-BCX. This number decreases to 2 for 2FXb-BCX. Similarly, seven residues in this region show significant motion on two widely different timescales (model 5) in apo-BCX, while no residues in 2FXb-BCX show this behavior. It is possible that increased noncovalent interactions between the residues forming the binding pocket of BCX and the substrate are responsible for the simpler motions in the residues in this region of the protein. Alternatively, as has been noted experimentally and theoretically (Schurr et al., 1994; Tjandra et al., 1995), neglect of self-association or anisotropic diffusion can erroneously lead to the calculation of terms reflecting the slower motions that appear in the isotropic models 3, 4, and 5. Interestingly, as discussed above, the longer τ_m of 2FXb-BCX may result from association due to small changes in sample pH and ionic strength, and global tumbling of this former of the protein may indeed be better fit by an axially symmetric diffusion model rather than one assuming isotropic tumbling. Despite these two potential difficulties, the relaxation data of 2FXb-BCX were more frequently fit to simple isotropic models than with apo-BCX. To better understand this observation, ^{15}N and ^{13}C relaxation studies at multiple field strengths, as well as $T_{1\rho}$ measurements, may be necessary.

BCX stability and dynamics

As shown by the ^{15}N relaxation results presented in this study, BCX is a well-ordered protein with very limited backbone flexibility on the sub-nanosecond timescale. Although the free energy of folding of BCX has not been determined due to problems of irreversible aggregation, it appears to be a relatively stable protein, as evidenced by an apparent midpoint unfolding temperature of ~60 °C at pH 5.5 and a midpoint urea denaturation concentration of 5.5 M at this same pH and 20 °C (L.P. McIntosh, unpubl. obs.). It is tempting to speculate that this global stability, which likely results from the enzyme's compact and extensively hydrogen-bonded β-sheet structure, correlates directly with the limited internal flexibility observed for the backbone of BCX. However, we note that the relationship between the global or local stability of a protein and its dynamic properties is probably complex due to the phenomenon of enthalpy–entropy compensation. That is, a protein molecule may be stabilized in its folded state by maximizing enthalpically favorable interactions (at the expense of rigid ordering and hence unfavorable entropy loss) or by minimizing entropically unfavorable changes relative to its unfolded state (at the expense of limiting enthalpic interactions).

Upon formation of the glycosyl-enzyme intermediate, the overall S^2 values of the amides in BCX increase slightly, indicating a possible, albeit very small, reduction in the mobility of the backbone of the protein on a fast timescale. In addition, based on the trend toward fitting the relaxation behavior of 2FXb-BCX with simpler motional models, mobility on the micro-to-millisecond timescale may also be dampened in the intermediate state. Although the effects of this modification on the global stability of BCX have not been defined in any detail due to the aforementioned problems of aggregation, preliminary measurements indicate that 2FXb-BCX is indeed more stable than the unmodified protein. For example, upon covalent modification with DNP-2FXb, the apparent midpoint unfolding temperature of BCX increases from ~60 to 65 °C at pH 4.0 and in 20% glycerol (v/w) (M. Korner, L.P. McIntosh, & S.G. Withers, unpubl. obs.). Given that the structures of apo- and 2FXb-BCX do not differ significantly, it is likely that the observed increase in resistance to proteolytic degradation upon complex formation (S.G. Withers, unpubl. obs.) reflects this increase in global stability, which leads to a reduction in the amplitude or frequency of

large-scale fluctuations of the protein that are required to expose segments of its backbone for attack by a protease. However, it is unclear how this stabilization is correlated with the relatively minor differences, if any, between the relaxation behavior observed between apo- and 2FXb-BCX. Furthermore, it is unlikely any changes in the backbone mobility of the enzyme on the sub-nanosecond timescale accounts for its increased resistance towards cleavage by proteases. This, of course, is not surprising, as the motions leading to NMR relaxation and proteolytic susceptibility are probably vastly different in amplitude and frequency. This highlights the need to characterize the dynamic properties of a protein by using a wide variety of techniques, including methods such as amide hydrogen exchange, to adequately sample the spectrum of relevant motional timescales.

BCX dynamics—Implications for the enzymatic mechanism

Despite numerous studies and methodological advances in recent years, the relationship between the internal motions of enzymes and their catalytic properties remains to be well defined. Conflicting data have been reported regarding the effects of protein–ligand binding and enzyme–substrate complex formation on protein motions for the timescales that can be investigated by ^{15}N relaxation studies. For example, complex formation has been shown to be accompanied by a decrease in the backbone order parameters of active-site residues in 4-oxalocrotonate tautomerase (Stivers et al., 1996), while studies on calbindin D_{9k} and a biotin carboxyl carrier protein show binding site regions that become more ordered upon interaction (Akke et al., 1993; Yao et al., 1999). Investigations of the *lac* repressor and the biotin carboxyl carrier protein subunit of acetyl-CoA carboxylase have also shown reductions in mobility of backbone amides due to complex formation (Kaptein et al., 1995; Yao et al., 1999). Several proteins even show distinct order parameter changes in both directions, such as dihydrofolate reductase (Epstein et al., 1995) and an SH2 domain of phospholipase (Farrow et al., 1994). The significance of these changes is as yet unclear, although it has been suggested that an increase in disorder for residues distal to a protein's binding site may help to offset the entropic penalty incurred when active-site residues become more ordered upon complex formation (Stivers et al., 1996).

In the case of BCX, the magnitude of any individual order parameter changes between its free and glycosyl-enzyme intermediate states is somewhat smaller than those reported for other proteins. We speculate that this is due to the high inherent conformational rigidity of BCX, even in the apo state. As BCX is a secreted enzyme, its lack of flexibility may be required for it to function in a harsh extracellular environment. In addition, BCX is not allosterically regulated; therefore, it does not need to contain flexible regions capable of responding structurally to the binding of an effector molecule. Finally, it is possible that the highly ordered structure of the protein is required to enable the distortion of the proximal sugar residue as seen in the crystal structure of 2FXb-BCX (Sidhu et al., 1999).

Materials and methods

Protein preparation

A single, uniformly $^{13}C/^{15}N$-labeled BCX sample, containing 0.9 mM protein in 25 mM sodium acetate-d_3, 0.02% sodium azide and 10% D_2O at pH 5.7, was used for all the assignment and relaxation experiments described in this paper. This was the same sample for which the ^1H, ^{13}C, and ^{15}N assignments for the apoprotein were determined (Plesniak et al., 1996b). Well after this initial NMR work was completed, it was discovered that two mutations, encoding Ser134 to Thr and Thr147 to Ser, had been introduced into the pCW expression plasmid during subcloning of the xylanase gene. The latter of these substitutions corresponds to that found in the homologous *B. subtilis* xylanase. Positions 134 and 147 are both located on the surface of the protein, and the amino acid substitutions do not change its structure or enzymatic activity (Campbell et al., 1993; Wakarchuk et al., 1994a). The NMR spectra of the mutant and wild-type forms of BCX are essentially identical. To remain consistent with previous work, the double-labeled protein in this paper is simply referred to as BCX (see also Connelly & McIntosh, 1998).

A mechanism-based inhibitor, 2,4-dinitrophenyl 2-deoxy-2-fluoro-β-xylobioside (DNP-2FXb), was synthesized as described previously (Ziser et al., 1995). The molecular weight of the unmodified $^{13}C/^{15}N$-labeled BCX was 21,545 ± 3 Da, as measured by electrospray mass spectrometry. After inactivation, the mass of 2FXb-BCX was determined to be 21,817 ± 3 Da. This difference is equal, within experimental error, to the mass of 2FXb (calculated: 267 Da), confirming that the enzyme forms a 1:1 complex with the mechanism-based inactivator.

NMR spectroscopy

The assignment and relaxation spectra used in this study were recorded with a Varian Unity spectrometer, operating at 500 MHz for protons and equipped with a pulsed-field gradient $^1H/^{13}C/^{15}N$ probe. All experiments were done at 30 °C. The ^1H spectral widths were 6,250 Hz, with the transmitter set at the frequency of H_2O (4.7 ppm). ^{15}N spectral widths were 1,575 Hz, centered at 121.4 ppm, and $^{13}C^{\alpha,\beta}$ spectral widths were 8,050 Hz, centered at 43 ppm, as described previously (Plesniak et al., 1996b).

The ^1H–^{15}N HSQC spectra used to measure ^{15}N T_1 and T_2, and $^{15}N\{^1H\}$ steady-state NOE values for the free and the bound protein were recorded with water-selective pulse sequences described in Farrow et al. (1994). The T_1 and T_2 HSQC spectra were collected with 96 complex points in the ^{15}N dimension and 800 (zero-filled to 2k) complex points in the ^1H dimension, with 24 transients accumulated for each t_1 increment. The T_1 series consisted of nine experiments, with delay times of 11.1, 33.2, 55.3, 99.5, 165.9, 287.6, 420.3, 608.3, and 940.1 ms. The T_2 series used CPMG delays of 16.8, 33.7, 50.5, 67.3, 84.1, 101.0, 117.8, 134,6, and 151.5 ms. To minimize experimental artifacts, the nine spectra in a given series were acquired in random order. Two $^{15}N\{^1H\}$ NOE spectra were recorded for each sample, one with a 5.0 s relaxation delay (control) and one with a 2.0 s relaxation delay followed by a 3.0 s proton presaturation period (NOE). These data sets were the same size as those for the T_1 and T_2 series, but recorded with 64 transients per increment.

After the first relaxation series was completed on the apo-BCX sample, 1 mg of DNP-2FXb was added to the 550 μL protein solution, giving approximately a fourfold molar excess of inactivator over enzyme. Three short (20 min) ^1H–^{15}N HSQC spectra were recorded in succession to monitor the formation of the covalently modified glycosyl-enzyme intermediate (2FXb-BCX). The third HSQC showed no evidence of signals from the free protein. This was confirmed by mass spectrometry. At this point, the same

^{15}N relaxation series was recorded on the sample. The protein remained fully in the 2FXb-BCX form throughout these measurements, as judged by its invariant NMR spectrum.

When the relaxation experiments were finished, several ^{1}H–^{13}C–^{15}N correlation spectra were recorded to enable the assignment of the ^{1}H–^{15}N cross peaks of 2FXb-BCX (Plesniak et al., 1996b). These were, in order, an HNCACB (Wittekind & Müeller, 1993), a CBCA(CO)NH (Grzesiek & Bax, 1992), and an H(CCO)NH (Grzesiek et al., 1993; Muhandiram & Kay, 1994). Between successive three-dimensional experiments, ^{1}H–^{15}N HSQC spectra were recorded to monitor the reappearance of peaks diagnostic of apo-BCX. After completion of the HNCACB, weak cross peaks from apo-BCX were detected in a ^{1}H–^{15}N HSQC spectrum, and thus an additional 1.0 mg of DNP-2FXb was added. The final pH of the sample decreased slightly to 5.4 due to the hydrolysis of DNP-2FXb by the protein.

Data processing

All spectra were processed as described in Plesniak et al. (1996b) using Felix software (Biosym, San Diego, California). The peak heights in the ^{15}N relaxation spectra were measured by fitting to optimized Lorentzian line shapes, using a routine developed in house by Emmanuel Brun. T_1 and T_2 values were determined by fitting peak heights for a given amide resonance to the equation

$$I(t) = I_0 \exp(-t/T_{1,2}) \quad (1)$$

with a program provided by Neil Farrow (University of Toronto). Errors in the fitted rates were estimated using a Monte Carlo procedure (Farrow et al., 1994). The ^{15}N{^{1}H} NOE data were also processed as detailed in Farrow et al. (1994).

Relaxation theory

^{1}H–^{15}N relaxation has been discussed in detail by others (Clore et al., 1990a, 1990b; Peng & Wagner, 1994), and, hence, only a brief overview is presented here. For a given peptide NH group, the three measured relaxation parameters (T_1, T_2, and the NOE) are functions of the spectral density, $J(\omega)$, at that position in the protein. The spectral density depends on the amplitudes and frequencies of any internal motions that may be occurring at that site, as well as the global tumbling time (τ_m) of the molecule. $J(\omega)$ is formally a function of five different frequencies: 0, ω_N, ω_H, $\{\omega_H - \omega_N\}$, and $\{\omega_H - \omega_N\}$. In the absence of any assumptions as to the form of $J(\omega)$, measurement of the three relaxation parameters T_1, T_2, and the NOE will always be insufficient to uniquely determine $J(\omega)$. The "model-free" formalism of Lipari and Szabo (1982a, 1982b) provides a suitable approximation for the spectral density, characterizing the internal motions of a particular ^{1}H–^{15}N bond vector in terms of a generalized order parameter (S^2) and an internal correlation time (τ_e).

$$J(\omega) = 2/5\,[S^2\tau_m/(1 + \omega^2\tau_m^2) + (1 - S^2)\,\tau/(1 + \omega^2\tau^2)] \quad (2)$$

where S^2 measures the degree of restriction of the motion and τ_e, contained in the relation $1/\tau = 1/\tau_m + 1/\tau_e$, reflects the rate of these motions. As outlined by Farrow et al. (1994), we first calculate a global τ_m, which best fits all the data. S^2 and τ_e are then optimized for each site separately. When $\tau_e \ll \tau_m$ for a given peptide group, Equation 2 reduces to

$$J(\omega) = 2/5\,[S^2\tau_m/(1 + \omega^2\tau_m^2)] \quad (3)$$

and only S^2 and the global τ_m are needed to adequately represent molecular motion at that site. For some NH groups, conformational exchange on the μs to ms timescale (represented as R_{ex}) can contribute significantly to the transverse relaxation process (T_2), along with the usual dipole–dipole and chemical shift anisotropy terms (R_2^{DD} and R_2^{CSA}, respectively):

$$1/T_2 = R_2^{DD} + R_2^{CSA} + R_{ex}. \quad (4)$$

In other cases, where significant intramolecular motions occur at a particular NH site on two different timescales (one near τ_m), the extended model-free analysis developed by Clore et al. (1990a, 1990b) can be applied to accurately fit the relaxation data. Here, the original order parameter S^2 is represented as a product of two order parameters, S_f^2 and S_s^2 (with corresponding time constants τ_f and τ_s) describing fast and slow internal motions, respectively. The equation for the spectra density then becomes

$$J(\omega) = 2/5\,[S^2\tau_m/(1 + \omega^2\tau_m^2) + (1 - S_f^2)\,\tau_1/(1 + \omega^2\tau_1^2) + (1 - S_s^2)\,\tau_2/(1 + \omega^2\tau_2^2)] \quad (5)$$

where τ_1 and τ_2 are defined by the relations $1/\tau_1 = 1/\tau_m + 1/\tau_f$ and $1/\tau_2 = 1/\tau_m + 1/\tau_s$.

Model selection

The internal motions at each backbone ^{1}H–^{15}N bond in BCX were fit with the simplest model using the fewest parameters necessary to explain the data, following the method of Farrow et al. (1994). These models are typically numbered 1–5, in order of increasing complexity (see Table 1). All depend on the calculated global correlation time τ_m. Model 1 uses only one other variable, the order parameter S^2, to explain the relaxation at a given site. Model 2 uses S^2 and incorporates a time constant (τ_e) measuring fast motions at the individual site. Chemical exchange and slow motions are assumed to be negligible. Model 3 employs S^2 and a parameter R_{ex} to quantify chemical exchange that may be occurring at the site as reflected by increased line widths. Motions on both the fast and slow timescales in this model at the site of the individual residue are assumed to be negligible. Model 4 includes all of the parameters S^2, τ_e, and R_{ex}. Model 5 assumes that motions are significant on two different timescales, and thus also uses a time constant for slower motions τ_s, and the accompanying order parameter (see Clore et al., 1990a, 1990b). A particular model was concluded to adequately describe the motions derived from the relaxation parameters if (1) each of the T_1, T_2, and the ^{15}N{^{1}H} NOE values could be fit to within a 95% confidence limit; and (2) the value of each fitting parameter in the model exceeded its calculated error. The simplest model (with the fewest parameters) meeting the above criteria was the one selected for a particular residue.

Acknowledgments

This work was funded by the Government of Canada's Network of Centres of Excellence Program supported by the Medical Research Council of Canada and the Natural Science and Engineering Research Council through PENCE Inc. We are grateful to Lewis Kay, Nico Tjandra, and Gary Sidhu for many insightful discussions, to Emmanuel Brun for providing the NMR peak-height measuring program, and to Niel Farrow and Arthur Palmer III for providing software for relaxation analysis. We also thank Kelly Joe Phelps for inspiration, and the Alexander von Humbolt-Stiftung for a Research Fellowship to L.P.M.

References

Akke M, Skelton NJ, Kördel J, Palmer AG III, Chazin WJ. 1993. Effects of ion binding on the backbone dynamics of calbindin D_{9k} determined by ^{15}N NMR relaxation. *Biochemistry 32*:9832–9844.

Anderson DE, Lu J, McIntosh LP, Dahlquist FW. 1993. The folding, stability and dynamics of T4 lysozyme: A perspective using nuclear magnetic resonance. In: Clore GM, Gronenborn AM, eds. *NMR of proteins*. London: MacMillan Press Ltd. pp 258–304.

Blackledge M, Cordier F, Dosset P, Marion D. 1998. Precision and uncertainty in the characterization of anisotropic rotational diffusion by ^{15}N relaxation. *J Am Chem Soc 120*:4538–4539.

Brüschweiler R, Liao X, Wright PE. 1995 Long-range motional restrictions in a multidomain zinc-finger protein from anisotropic tumbling. *Science 268*:886–889.

Burmeister WP, Cottaz S, Driguez H, Iori R, Palmieri S, Henrissat B. 1997. The crystal structures of *Sinapis alba* myrosinase and a covalent glycosyl-enzyme intermediate provide insights into the substrate recognition and active-site machinery of an S-glycosidase. *Structure 5*:663–675.

Campbell RL, Rose DR, Wakarchuk WW, To R, Sung W, Yaguchi M. 1993. A comparison of the structures of the 20 kDa xylanases from *Trichoderma harzianum* and *Bacillus circulans*. In: Suominen P, Reinikainen T, eds. *Proceedings of the second TRICEL symposium on* Trichoderma reesei *cellulases and other hydrolases*. Helsinki, Finland: Foundation for Biotechnical and Industrial Fermentation Research. pp 63–72.

Cavanagh J, Fairbrother WJ, Palmer AG III, Skelton NJ. 1996. *Protein NMR spectroscopy: Principles and practice*. San Diego: Academic Press. pp 16–19.

Clore GM, Driscoll PC, Wingfield PT, Gronenborn AM. 1990a. Analysis of the backbone dynamics of interleukin-1β using two-dimensional inverse detected heteronuclear ^{15}N-^{1}H NMR spectroscopy [published erratum appears in *Biochemistry 30*(1):312, 1991]. *Biochemistry 29*:7387–7401.

Clore GM, Szabo A, Bax A, Kay LE, Driscoll PC, Gronenborn AM. 1990b. Deviations from the simple two-parameter model-free approach to the interpretation of nitrogen-15 nuclear magnetic relaxation of proteins. *J Am Chem Soc 112*:4989–4991.

Clubb RT, Omichinski JG, Sakaguchi K, Appella E, Gronenborn AM, Clore GM. 1995. Backbone dynamics of the oligomerization domain of p53 determined from ^{15}N NMR relaxation measurements. *Protein Sci 4*:855–862.

Connelly GP, McIntosh LP. 1998. Characterization of a buried neutral histidine in *Bacillus circulans* xylanase: Internal dynamics and interaction with a bound water molecule. *Biochemistry 37*:1810–1818.

Davies GJ, Mackenzie L, Varrot A, Dauter M, Brzozowski AM, Schulein M, Withers SG. 1998. Snapshots along an enzymatic reaction coordinate: Analysis of a retaining β-glycoside hydrolase. *Biochemistry 37*:11707–11713.

Epstein DM, Benkovic SJ, Wright PE. 1995. Dynamics of the dihydrofolate reductase-folate complex: Catalytic sites and regions known to undergo conformational change exhibit diverse dynamical features. *Biochemistry 34*:11037–11048.

Farrow NA, Muhandiram R, Singer AU, Pascal SM, Kay CM, Gish G, Shoelson SE, Pawson T, Forman-Kay JD, Kay LE. 1994. Backbone dynamics of a free and a phosphopeptide-complexed Src Homology 2 domain studied by ^{15}N NMR relaxation. *Biochemistry 33*:5984–6003.

Gebler J, Gilkes NR, Claeyssens M, Wilson DB, Béguin P, Wakarchuk WW, Kilburn DG, Miller RCJ, Warren RA, Withers SG. 1992. Stereoselective hydrolysis catalyzed by related beta-1,4-glucanases and beta-1,4-xylanases. *J Biol Chem 267*:12559–12561.

Grzesiek S, Bax A. 1992. Correlating backbone amide and side chain resonances in larger proteins by multiple relayed triple resonance NMR. *J Am Chem Soc 114*:6291–6293.

Grzesiek S, Anglister J, Bax A. 1993. Correlation of backbone amide and aliphatic side-chain resonances in $^{13}C/^{15}N$ proteins by isotropic mixing of ^{13}C magnetization. *J Magn Reson Series B 101*:114–119.

Joshi MD, Hedberg A, McIntosh LP. 1997. Complete measurement of the pK_a values of the carboxyl and imidazole groups in *Bacillus circulans* xylanase. *Protein Sci 6*:2667–2670.

Kaptein R, Slijper M, Boelens R. 1995. Structure and dynamics of the *lac* repressor-operator complex as determined by NMR. *Toxicol Lett 82/83*:591–599.

Kay LE, Muhandiram DR, Wolf G, Shoelson SE, Forman-Kay JD. 1998. Correlation between binding and dynamics at SH2 domain interfaces. *Nat Struct Biol 5*:156–163.

Kay LE, Torchia DA, Bax A. 1989. Backbone dynamics of proteins as studied by ^{15}N inverse detected heteronuclear NMR spectroscopy: Application to staphylococcal nuclease. *Biochemistry 28*:8972–8979.

Krengel U, Dijkstra BW. 1996. Three-dimensional structure of endo-1,4-β-xylanase I from *Aspergillus niger*: Molecular basis for its low pH optimum. *J Mol Biol 263*:70–78.

Lawson SL, Wakarchuk WW, Withers SG. 1996. Effects of both shortening and lengthening the active site nucleophile of *Bacillus circulans* xylanase on catalytic activity. *Biochemistry 35*:10110–10118.

Lawson SL, Wakarchuk WW, Withers SG. 1997. Positioning the acid/base catalyst in a glycosidase: Studies with *Bacillus circulans* xylanase. *Biochemistry 36*:2257–2265.

Lee L, Rance M, Chazin WJ, Palmer AG III. 1997. Rotational diffusion anisotropy of proteins from simultaneous analysis of ^{15}N and ^{13}C nuclear spin relaxation. *J Biomol NMR 9*:287–298.

Lipari G, Szabo A. 1982a. Model-free approach to the interpretation of nuclear magnetic resonance relaxation in macromolecules. 1. Theory and range of validity. *J Am Chem Soc 104*:4546–4559.

Lipari G, Szabo A. 1982b. Model-free approach to the interpretation of nuclear magnetic resonance relaxation in macromolecules. 2. Analysis of experimental results. *J Am Chem Soc 104*:4559–4570.

Mandel AM, Akke M, Palmer AG III. 1995. Backbone dynamics of *Escherichia coli* ribonuclease HI: Correlations with structure and function in an active enzyme. *J Mol Biol 246*:144–163.

McDonald IK, Thornton JM. 1994. Satisfying hydrogen bonding potential in proteins. *J Mol Biol 238*:777–793.

McIntosh LP, Hand G, Johnson PE, Joshi MD, Korner M, Plesniak LA, Ziser L, Wakarchuk WW, Withers SG. 1996. The pK_a of the general acid/base carboxyl group of a glycosidase cycles during catalysis: A ^{13}C-NMR study of *Bacillus circulans* xylanase. *Biochemistry 35*:9958–9966.

Miao S, Ziser L, Aebersold R, Withers SG. 1994. Identification of glutamic acid 78 as the active site nucleophile in *Bacillus subtilis* xylanase using electrospray tandem mass spectroscopy. *Biochemistry 33*:7027–7032.

Muhandiram DR, Kay LE. 1994. Gradient-enhanced triple-resonance three-dimensional NMR experiments with improved sensitivity. *J Mag Res 103 (Series B)*:203–216.

Notenboom V, Birsan C, Warren RAJ, Withers SG, Rose DR. 1998. Exploring the cellulose/xylan specificity of the β-1,4-glycanase Cex from *Cellulomonas fimi* through crystallography and mutation. *Biochemistry 37*:4751–4758.

Olejniczak ET, Zhou M-M, Fesik SW. 1997. Changes in the NMR-derived motional parameters of the insulin receptor substrate 1 phosphotyrosine binding domain upon binding to an interleukin 4 receptor phosphopeptide. *Biochemistry 36*:4118–4124.

Peng JW, Wagner G. 1992a. Mapping of the spectral densities of N-H bond motions in eglin c using heteronuclear relaxation experiments. *Biochemistry 31*:8571–8586.

Peng JW, Wagner G. 1992b. Mapping spectral density functions using heteronuclear NMR relaxation measurements. *J Mag Res 98*:308–332.

Peng JW, Wagner G. 1994. Investigation of protein motions via relaxation measurements. *Methods Enzymol 239*:563–596.

Plesniak LA, Connelly GP, Wakarchuk WW, McIntosh LP. 1996a. Characterization of a buried neutral histidine residue in *Bacillus circulans* xylanase: NMR assignments, pH titration and hydrogen exchange. *Protein Sci 5*:2319–2328.

Plesniak LA, Wakarchuk WW, McIntosh LP. 1996b. Secondary structure and NMR assignments of *Bacillus circulans* xylanase. *Protein Sci 5*:1118–1135.

Rischel C, Madsen JC, Andersen KV, Poulsen FM. 1994. Comparison of backbone dynamics of *apo*- and *holo*-acyl-coenzyme A binding protein using ^{15}N relaxation measurements. *Biochemistry 33*:13997–14002.

Schurr MJ, Babcock HP, Fujimoto BS. 1994. A test of the model-free formulas. Effects of anisotropic rotational diffusion and dimerization. *J Mag Res 105B*:211–224.

Sidhu G, Withers SG, Nguyen NT, McIntosh LP, Ziser L, Brayer GD. 1999. Sugar ring distortion in the glycosyl-enzyme intermediate of a family G/11 xylanase. *Biochemistry 38*:5346–5354.

Stivers JT, Abeygunawardana C, Mildvan AS. 1996. ^{15}N NMR relaxation studies of free and inhibitor-bound 4-oxalocrotonate tautomerase: Backbone dynamics and entropy changes upon inhibitor binding. *Biochemistry 35*:16036–16047.

Street IP, Kempton JB, Withers SG. 1992. Inactivation of a β-glucosidase through the accumulation of a stable 2-deoxy-2-fluoro-α-D-glucopyranosyl-enzyme intermediate: A detailed investigation. *Biochemistry 31*:9970–9978.

Tjandra N, Feller SE, Pastor RW, Bax A. 1995. Rotational diffusion anisotropy of human ubiquitin from ^{15}N relaxation. *J Am Chem Soc 117*:12562–12566.

Törrönen A, Harkki A, Rouvinen J. 1994. Three-dimensional structure of endo-1,4-β-xylanase II from *Trichoderma reesei*: Two conformational states in the active site. *EMBO J 13*:2943–2501.

Törrönen A, Rouvinen J. 1995. Structural comparison of two major endo-1,4-xylanases from *Trichoderma reesei*. *Biochemistry 34*:847–856.

Törrönen A, Rouvinen J. 1997. Structural and functional properties of low molecular weight endo-1,4-β-xylanases. *J Biotechnol 57*:137–149.

Wakarchuk WW, Campbell RL, Sung WL, Davoodi J, Yaguchi M. 1994a. Mutational and crystallographic analysis of the active site residues of the *Bacillus circulans* xylanase. *Protein Sci 3*:467–475.

Wakarchuk WW, Sung WL, Campbell RL, Cunningham A, Watson DC, Yaguchi M. 1994b. Thermostabilization of the *Bacillus subtilis* xylanase by the introduction of disulfide bonds. *Protein Eng 7*:1379–1386.

White A, Rose DR. 1997. Mechanism of catalysis by retaining β-glycosyl hydrolases. *Curr Opin Struct Biol 7*:645–651.

White A, Tull D, Johns K, Withers SG, Rose DR. 1996. Crystallographic observation of a covalent catalytic intermediate in a β-glycosidase. *Nat Struct Biol 3*:149–154.

Wittekind M, Müeller L. 1993. HNCACB, a high-sensitivity 3D NMR experiment to correlate amide-proton and nitrogen resonances with the alpha- and beta-carbon resonances. *J Mag Res 101 (Series B)*:201–205.

Yao X, Soden CJ, Summers MF, Beckett D. 1999. Comparison of the backbone dynamics of the apo- and holo-carboxy-terminal domain of the biotin carboxyl carrier subunit of *Escherichia coli* acetyl-CoA carboxylase. *Protein Sci 8*:307–317.

Zink T, Ross A, Luers K, Cieslar C, Rudolph R, Holak TA. 1994. Structure and dynamics of the human granulocyte colony-stimulating factor determined by NMR spectroscopy. Loop mobility in a four-helix-bundle. *Biochemistry 33*:8453–8463.

Ziser L, Setyawati I, Withers SG. 1995. Syntheses and testing of substrates and mechanism-based inactivators for xylanases. *Carbohydrate Res 274*:137–153.